
Time - Dependent Magnetohydrodynamic Non-Newtonian Nanofluid Flow with Lorentz Force, Viscous Dissipation and Thermophoresis Between Parallel Plates

Kafunda Tuesday^{1, *}, Mukonda Danny¹, Mwamba Nictor², Levy Kahyata Matindih¹,
Chenjelani Mwale¹, Stanley Jere¹

¹Department of Mathematics and Statistics, Mulungushi University, Kabwe, Zambia

²Department of Applied Sciences and Engineering, Eden University, Lusaka, Zambia

Email address:

kaftuz25@gmail.com (Kafunda Tuesday), dmukonda@mu.edu.zm (Mukonda Danny), nictormk@gmail.com (Mwamba Nictor),

kahyamatindih99@gmail.com (Levy Kahyata Matindih), mwalechenje@gmail.com (Chenjelani Mwale), sjere@mu.edu.zm (Stanley Jere)

*Corresponding author

To cite this article:

Kafunda Tuesday, Mukonda Danny, Mwamba Nictor, Levy Kahyata Matindih et al. (2024). Time - Dependent Magnetohydrodynamic Non-Newtonian Nanofluid Flow with Lorentz Force, Viscous Dissipation and Thermophoresis Between Parallel Plates. *Applied and Computational Mathematics*, 13(6), 224-235. <https://doi.org/10.11648/j.acm.20241306.12>

Received: 26 July 2024; **Accepted:** 6 November 2024; **Published:** 18 December, 2024

Abstract: The study examined a three-dimensional unsteady Magnetohydrodynamic non-Newtonian nanofluid flow with magnetic induction, Lorentz force, viscous dissipation and thermophoresis between two parallel horizontal plates. In this study, fluid's dynamic viscosity and thermal conductivity parameters have been assumed to vary depending on temperature changes. The density has been assumed to be incompressible and also the study assumes that the gravitational effects are negligible. The governing equations: continuity, Navier-Stokes, Energy, Magnetic Induction and Concentration equations for the non-Newtonian nanofluid flow have been developed and non-dimensionalized. Dimensionless parameters arising from the dimensionless equations have also been determined. Finite difference numerical approximation method has been used to approximate the systems of the governing equations in difference form. Profiles for the flow variables have been presented and discussed. Results show that increasing thermophoresis parameter increases the specie concentration while increasing Schmidt number and chemical reaction parameter reduces concentration profiles. Magnetic induction profiles rise with an increase in Reynolds number but declines with an increase in magnetic Prandtl number. Temperature and velocity profiles increase with an increase in Reynolds number. The study of electrically conducting fluids with the consideration of Lorentz force, thermophoresis, viscous dissipation, chemical reaction, variable dynamic viscosity, variable thermal conductivity and magnetic induction is very useful in designing heat and mass transfer appliances. It is also significant in cooling and overheating control systems.

Keywords: Unsteady, Magnetohydrodynamic, Non-Newtonian, Nanofluid, Magnetic Induction, Lorentz Force, Viscous Dissipation, Thermophoresis

1. Introduction

Studies on fluid flows between parallel plates have attracted attention by many researchers. [1] investigated the steady flow of an electrically conducting, viscous, incompressible fluid bounded by two parallel infinite insulated horizontal plates and the heat transfer through it. The upper plate was given a constant velocity while the lower plate was kept

stationary. The viscosity of the fluid was assumed to vary with temperature. The effect of an external uniform magnetic field as well as the action of an inflow perpendicular to the plates together with the influence of the pressure gradient on the flow and temperature distributions were presented and discussed. A numerical solution for the governing non-linear ordinary differential equations was developed.

Analysis of the problem of unsteady squeezing flow of a

non-Newtonian nanofluid through a porous medium between two parallel plates was conducted [2]. The effects of Hall currents and heat source were taken into consideration. The governing partial differential equations are transformed into a set of nonlinear ordinary differential equations by using similarity transformations. A homotopy perturbation method is performed to obtain analytical solutions for that system of equations. The behaviors of the tangential velocity, normal velocity, temperature, and nanoparticles concentrations distributions were discussed analytically and graphically under the effect of different entering parameters.

Nanofluids have attained a big consideration from scientists because of their enriched heat transfer properties. Thickness shows a vigorous part in the effectiveness of nanofluids in the convection progressions as well. [3] planned the rheological performance of a graphene nanofluid via rotating rheometer. [4] also examined the rheological possessions of 6 carbon-based nanofluids. Currently, nanofluids are categorized as hybrid nanofluids in various modules [5]. Hybrid nanofluids become by combining two distinct nanoparticles in base fluid. The key motivation of it is to moreover advance thermal features of nanofluids. A study on adjustable heat transmission of hybrid nanofluid under the influence of outer magnetic field was carried out. This study dealt with the CFD simulation of natural convection heat transfer of a hybrid nanofluid in an inverted T-shaped cavity partitioned and saturated by two different types of porous media [6]. Suspensions of organic and inorganic nanoparticles, i.e., MWCNTs and Fe_3O_4 , in water were selected as the working fluid. The macroscopic conservation equations for the flow field and heat transfer were modeled via volume averaging the microscopic equations inside porous media over a representative elementary volume. The effects of many parameters were investigated. The results showed that, with an increase in the Rayleigh number, porosity ratio and Darcy number ratio and decrease in the thermal conductivity ratio, the averaged Nusselt number increased.

Investigation of the innovative heat transfer in non-Newtonian hybrid nanofluid collected with entropy group was conducted. The study investigated the effects of concentration and radius ratio on convective heat transfer and entropy generation of a non-Newtonian hybrid nanofluid flowing through a concentric annulus [7]. The nanofluid was prepared by suspending tetramethylammonium hydroxide (TMAH) coated Fe_3O_4 (magnetite) nanoparticles and gum arabic (GA) coated carbon nanotubes (CNTs) in water. Variable thermal conductivity and viscosity are used in simulations. [8] examined the impact of unsteady viscous flow in a squeezing channel. Silver-Cgold hybrid nanofluid particles with different shapes were inserted in the base fluid engine oil. Flow and heat transfer mechanism were detected in the presence of magnetohydrodynamics between the two parallel infinite plates. The thermal conductivity models, that is, Yamada-COTA and Hamilton-CCrosser models were used to investigate various shapes (Blade, platelet, cylinder, and brick) of hybrid nanoparticles. The model was made up of paired high nonlinear partial differential equations that were then transformed into ordinary differential equations which

are coupled and strong nonlinear using the boundary layer approximation.

Additionally, the analysis showed that the Yamada-COTA model of the Hybrid nanofluid gains high temperature and velocity profile than the Hamilton-CCrosser model of the hybrid nanofluid. Also, both the models showed increasing trends toward increasing the volume fraction rate of silver-gold hybrid nanoparticles. It was also observed that the hybrid-nanoparticles performance was far better than the common nanofluids. [9] investigated the flow and heat transfer of Magnetohydrodynamic squeezing nanofluid flow between two infinite parallel plates had been investigated. The fluid used was an equal mixture of Ethylene-glycol and water. This paper discusses the hybrid nanoparticle while articles were Fe_3O_4 and MoS_2 . The nonlinear equations have been solved by Akbari- Ganji's method. The effect of Harman number, base fluid, squeeze number, and Heat source on flow and heat transfer have been computed. The result shows that the Akbari- Ganji's method and the numerical method were in good agreement. Akbari- Ganji's method can be useful for such problems, and we can see that the maximum difference in velocity profile and thermal profile between AGM and the numerical method was less than one percent.

The findings showed that velocity profile reduced by an increase in squeeze number and Hartman number. The thermal profile raised with an increase in squeeze number, but it decreased with increasing in Hartman number and heat source parameter. [10] studied the impacts of viscous dissipation, thermal radiation and Joule heating on squeezing flow current and the heat transfer mechanism for a magnetohydrodynamic (MHD) nanofluid flow in parallel disks during a suction/blowing process. First, the governing momentum and energy equations were transformed into a non-dimensional form and then the obtained equations were solved by modified Adomian decomposition method (ADM), known as Duan-Rach approach (DRA).

In addition, the effects of the radiation parameter, suction/blowing parameter, magnetic parameter, squeezing number and nanoparticles concentration on the heat transfer and flow field were investigated in the results. The results showed that the fluid velocity increased with increasing suction parameter, while the temperature profile decreases with increasing suction parameter. [11] natural convection of non-Newtonian bio-nanofluids flow between two vertical flat plates was investigated numerically. Sodium Alginate (SA) and Sodium Carboxymethyl Cellulose (SCMC) are considered as the base non-Newtonian fluid, and nanoparticles such as Titania (TiO_2 and Alumina (Al_2O_3 were added to them.

The effective thermal conductivity and viscosity of nanofluids were calculated through Maxwell-Garnetts (MG) and Brinkman models, respectively. A fourth-order Runge-Kutta numerical method (RKNM) and three Weighted Residual Methods (WRMs), Collocation (CM), Galerkin (GM) and Least-Square Method (LSM) and Finite-Element Method (FEM), were used to solve the present problem. The influence of some physical parameters such as nanofluid volume fraction on non-dimensional velocity and temperature

profiles were discussed. The results show that SCMC- TiO_2 had higher velocity and temperature values than other nanofluid structures.

2. Mathematical Formulation

Figure 1 shows the physical configuration of the non-Newtonian nanofluid flow between two parallel horizontal plates in three dimensions. By the no-slip boundary condition,

at time $t \leq 0$, for $0 \leq (y, z) \leq h$, the nanofluid flow variables $v(y, z, 0) = 0$, $w(y, z, 0) = 0$, $T(y, z, 0) = T_{sp}$, $C = C_{sp}$, $H_y(y, z, 0) = 0$ and $H_z(y, z, 0) = 0$. When the nanofluid gets in contact with the moving plate at anytime $t > 0$, the flow variables $v(0, 0, t) = V_\infty$, $w(0, 0, t) = V_\infty$, $T(0, 0, t) = T_{mp}$, $C(0, 0, t) = C_{mp}$, $H_y(0, 0, t) = H_m$ and $H_z(0, 0, t) = H_m$ for $(y, z) = 0$. When $(y, z) = h$, the flow variables $v(y, z, t) = 0$, $w(y, z, t) = 0$, $T(y, z, t) = T_{sp}$, $C(y, z, t) = C_{sp}$, $H_y(y, z, t) = 0$ and $H_z(y, z, t) = 0$.

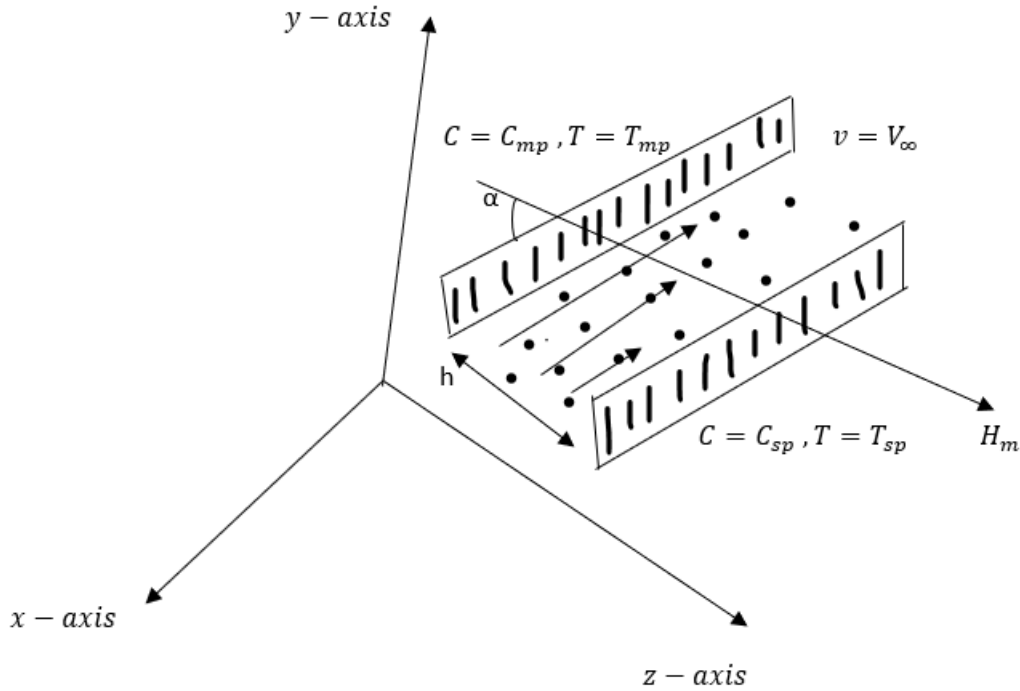


Figure 1. Physical Configuration of the Flow.

3. Governing Equations

Assuming that velocity of the fluid flow along x-axis is very small compared to the velocities in y and z -axes, then $u \rightarrow 0$. Thus,

$$\frac{\partial u}{\partial x} = 0 \quad (1)$$

This implies that the flow variables are independent of x but only depends on y, z and time t .

3.1. Continuity Equation

$$\frac{\partial v}{\partial y} + \frac{\partial w}{\partial z} = 0 \quad (2)$$

3.2. Navier-Stokes equation along x-axis

$$\frac{\partial u}{\partial t} + v \frac{\partial u}{\partial y} + w \frac{\partial u}{\partial z} = -\frac{\partial P}{\partial x} + \frac{\mu_\infty}{\rho_{nf} (1 + \delta (T - T_{sp}))} \left(\frac{\partial^2 u}{\partial y^2} + \frac{\partial^2 u}{\partial z^2} \right)$$

3.3. Navier-Stokes equation along y-axis

$$\begin{aligned} \frac{\partial v}{\partial t} + v \frac{\partial v}{\partial y} + w \frac{\partial v}{\partial z} = -\frac{\partial P}{\partial y} + \frac{\mu_{\infty}}{\rho_{n_f} (1 + \delta (T - T_{sp}))} \left(\frac{\partial^2 v}{\partial y^2} + \frac{\partial^2 v}{\partial z^2} \right) + B_t g (T - T_{sp}) + B_c g (C - C_{sp}) \\ - \sigma \mu_e^2 \left[\left(\vec{H}_m \sin \alpha + \vec{H}_y \right) v - \left(\vec{H}_m \cos \alpha + \vec{H}_z \right) w \right] \left(\vec{H}_m \sin \alpha + \vec{H}_y \right) \end{aligned} \quad (3)$$

3.4. Navier-Stokes equation along z-axis

$$\begin{aligned} \frac{\partial w}{\partial t} + v \frac{\partial w}{\partial y} + w \frac{\partial w}{\partial z} = -\frac{\partial P}{\partial z} + \frac{\mu_{\infty}}{\rho_{n_f} (1 + \delta (T - T_{sp}))} \left(\frac{\partial^2 w}{\partial y^2} + \frac{\partial^2 w}{\partial z^2} \right) \\ + \sigma \mu_e^2 \left[\left(\vec{H}_m \sin \alpha + \vec{H}_y \right) v - \left(\vec{H}_m \cos \alpha + \vec{H}_z \right) w \right] \left(\vec{H}_m \cos \alpha + \vec{H}_z \right) \end{aligned} \quad (4)$$

$$-\frac{\partial P}{\partial x} = -\frac{\partial(\rho_{n_f} g x)}{\partial x} = 0 \quad (5)$$

$$-\frac{\partial P}{\partial y} = -\frac{\partial(\rho_{n_f} g y)}{\partial y} = -\rho_{n_f} g \quad (6)$$

$$-\frac{\partial P}{\partial z} = -\frac{\partial(\rho_{n_f} g z)}{\partial z} = 0 \quad (7)$$

3.5. Equation of Energy

$$\begin{aligned} \frac{\partial T}{\partial t} + v \frac{\partial T}{\partial y} + w \frac{\partial T}{\partial z} = \frac{k_{\infty}}{\rho_{n_f} c_p} \left[1 + \epsilon \left(\frac{T - T_{sp}}{T_{mp} - T_{sp}} \right) \right] \left(\frac{\partial^2 T}{\partial y^2} + \frac{\partial^2 T}{\partial z^2} \right) + \\ \frac{\mu_{\infty}}{\rho_{n_f} c_p (1 + \delta (T - T_{\infty}))} \left(4 \left(\frac{\partial u}{\partial y} \right)^2 + \left(\frac{\partial v}{\partial z} + \frac{\partial w}{\partial y} \right)^2 \right) + \frac{\sigma \mu_e^2 \left[\left(\vec{H}_m \sin \alpha + \vec{H}_y \right) v - \left(\vec{H}_m \cos \alpha + \vec{H}_z \right) w \right]^2}{\rho_{n_f} c_p} \end{aligned} \quad (8)$$

3.6. Magnetic Induction Equation along x-axis

$$\frac{\partial \vec{H}_x}{\partial t} = 0 \quad (9)$$

3.7. Magnetic Induction Equation along y-axis

$$\frac{\partial \vec{H}_y}{\partial t} = \left(\vec{H}_m \sin \alpha + \vec{H}_y \right) \frac{\partial v}{\partial z} - \left(\vec{H}_m \cos \alpha + \vec{H}_z \right) \frac{\partial w}{\partial z} + v \frac{\partial \vec{H}_y}{\partial z} + \frac{1}{\mu_e \sigma} \left(\frac{\partial^2 \vec{H}_z}{\partial y^2} + \frac{\partial^2 \vec{H}_z}{\partial z^2} \right) \quad (10)$$

3.8. Magnetic Induction Equation along z-axis

$$\frac{\partial \vec{H}_z}{\partial t} = \left(\vec{H}_m \cos \alpha + \vec{H}_z \right) \frac{\partial w}{\partial y} - \left(\vec{H}_m \sin \alpha + \vec{H}_y \right) \frac{\partial v}{\partial y} - v \frac{\partial \vec{H}_y}{\partial y} + \frac{1}{\mu_e \sigma} \left(\frac{\partial^2 \vec{H}_y}{\partial y^2} + \frac{\partial^2 \vec{H}_y}{\partial z^2} \right) \quad (11)$$

3.9. Equation of Concentration

$$\frac{\partial C}{\partial t} = D_m \left(\frac{\partial^2 C}{\partial y^2} + \frac{\partial^2 C}{\partial z^2} \right) - v \frac{\partial C}{\partial y} - w \frac{\partial C}{\partial z} + \frac{D_m K_t}{T_m} \left(\frac{\partial^2 T}{\partial y^2} + \frac{\partial^2 T}{\partial z^2} \right) - k_r (C - C_\infty) \quad (12)$$

3.10. Initial and Boundary Conditions

The above equations are subject to the following initial and boundary conditions [12]:

Initial conditions

$$t \leq 0 : v = 0, w = 0, T = T_{sp}, C = C_{sp}, H_y = H_z = 0, 0 \leq y, z \leq h \quad (13)$$

Boundary conditions

$$t > 0 : \left\{ \begin{array}{ll} v = V_\infty, w = V_\infty, T = T_{mp}, C = C_{mp}, H_y = H_z = H_m & (y, z) = 0 \\ v = 0, w = 0, T = T_{sp}, C = C_{sp}, H_y = H_z = 0 & (y, z) = h \end{array} \right\} \quad (14)$$

4. Non-Dimensionalization Process

The following non-dimensional variables have been used for the present hydromagnetic flow problem

$$H_y = H^* H_m, H_z = H_z^* H_m, y = h y^*, z = h z^*, \\ t = \frac{h^2 t^*}{\nu_{nf}}, w = V_\infty w^*, v = V_\infty v^*, T = T_{sp} + (T_{mp} - T_{sp}) T^*, C = C_{sp} + (C_{mp} - C_{sp}) C^* \quad (15)$$

where V_∞ represents velocity of the moving plate, (y^*, z^*) represent dimensionless cartesian coordinates, H^* represents non-dimensional induced magnetic field, C^* represents non-dimensional concentration, ν_{nf} represents kinematic viscosity, T^* represents non-dimensional temperature, v^*, w^* represent non-dimensional velocity along y and z directions respectively and h is the distance between the two plates [12].

For easy writing, let $v^* = v, w^* = w, H^* = H, T^* = T, C^* = C, y^* = y$ and $z^* = z$.

4.1. Continuity Equation

$$\frac{\partial v}{\partial y} + \frac{\partial w}{\partial z} = 0 \quad (16)$$

4.2. Navier-Stokes equation along y-axis

$$\frac{\partial v}{\partial t} + Re.v \frac{\partial v}{\partial y} + Re.w \frac{\partial v}{\partial z} = \frac{\partial^2 v}{\partial y^2} + \frac{\partial^2 v}{\partial z^2} - M. \left[\left(\sin \alpha + \vec{H}_y \right) v - \left(\cos \alpha + \vec{H}_z \right) w \right] \left(\sin \alpha + \vec{H}_y \right) \quad (17)$$

4.3. Navier-Stokes equation along z-axis

$$\frac{\partial w}{\partial t} + Re.v \frac{\partial w}{\partial y} + Re.w \frac{\partial w}{\partial z} = \frac{\partial^2 w}{\partial y^2} + \frac{\partial^2 w}{\partial z^2} + M. \left[\left(\sin \alpha + \vec{H}_y \right) v - \left(\cos \alpha + \vec{H}_z \right) w \right] \left(\cos \alpha + \vec{H}_z \right) \quad (18)$$

4.4. Equation of Energy

$$\frac{\partial T}{\partial t} + Re.v \frac{\partial T}{\partial y} + Re.w \frac{\partial T}{\partial z} = \frac{1}{Pr} \left(\frac{\partial^2 T}{\partial y^2} + \frac{\partial^2 T}{\partial z^2} \right) + \\ E_c \left(4 \left(\frac{\partial u}{\partial y} \right)^2 + \left(\frac{\partial v}{\partial z} + \frac{\partial w}{\partial y} \right)^2 \right) + M.E_c \left[\left(\sin \alpha + \vec{H}_y \right) v - \left(\cos \alpha + \vec{H}_z \right) w \right]^2 \quad (19)$$

4.5. Magnetic Induction Equation along x-axis

$$\frac{\partial \vec{H}_x}{\partial t} = 0 \quad (20)$$

4.6. Magnetic Induction Equation along y-axis

$$\frac{\partial \vec{H}_y}{\partial t} = Re. \left(\sin \alpha + \vec{H}_y \right) \frac{\partial v}{\partial z} - Re. \left(\cos \alpha + \vec{H}_z \right) \frac{\partial w}{\partial z} + Re.v \frac{\partial \vec{H}_y}{\partial z} + \frac{1}{P_{rm}} \left(\frac{\partial^2 \vec{H}_z}{\partial y^2} + \frac{\partial^2 \vec{H}_z}{\partial z^2} \right) \quad (21)$$

4.7. Magnetic Induction Equation along z-axis

$$\frac{\partial \vec{H}_z}{\partial t} = Re. \left(\cos \alpha + \vec{H}_z \right) \frac{\partial w}{\partial y} - Re. \left(\sin \alpha + \vec{H}_y \right) \frac{\partial v}{\partial y} - Re.v \frac{\partial \vec{H}_y}{\partial y} + \frac{1}{P_{rm}} \left(\frac{\partial^2 \vec{H}_y}{\partial y^2} + \frac{\partial^2 \vec{H}_y}{\partial z^2} \right) \quad (22)$$

4.8. Equation of Concentration

$$\frac{\partial C}{\partial t} = \frac{1}{S_c} \left(\frac{\partial^2 C}{\partial y^2} + \frac{\partial^2 C}{\partial z^2} \right) - Re.v \frac{\partial C}{\partial y} - Re.w \frac{\partial C}{\partial z} + S_r \left(\frac{\partial^2 T}{\partial y^2} + \frac{\partial^2 T}{\partial z^2} \right) - \gamma C \quad (23)$$

4.9. Non-dimensional Initial and Boundary Conditions

The above equations are subject to the following initial and boundary conditions [12,13,14]:

Initial conditions

$$t \leq 0 : v = 0, w = 0, T = 0, C = 0, H_y = H_z = 0, 0 \leq (y, z) \leq 1 \quad (24)$$

Boundary conditions

$$t > 0 : \left\{ \begin{array}{ll} w = 1, v = 1, T = 1, C = 1, H_y = H_z = 1 & (y, z) = 0 \\ v = 0, w = 0, T = 0, C = 0, H_y = H_z = 0 & (y, z) = 1 \end{array} \right\} \quad (25)$$

5. Finite Difference Form of the Governing Equations

Finite difference approximation method has been used to approximate non-linear partial differential equations in terms of algebraic difference expressions which have been simulated in MATLAB. The step-sizes for the space coordinates and time are $\Delta t = 0.00001$ and $\Delta y = \Delta z = 0.02$ respectively [12,13,14].

5.1. Navier-Stokes Equation along y-axis

$$\begin{aligned} v_j^{k+1} = & v_j^k - Re.v.\Delta t \frac{v_{j+1}^k - v_{j-1}^k}{2\Delta y} - Re.w.\Delta t \frac{v_{j+1}^k - v_{j-1}^k}{2\Delta z} + \frac{v_{j+1}^k - 2v_j^k + v_{j-1}^k}{(\Delta y)^2} + \\ & \frac{v_{j+1}^k - 2v_j^k + v_{j-1}^k}{(\Delta z)^2} - M. \left[\left(\sin \alpha + \vec{H}_{y_j}^k \right) v_j^k - \left(\cos \alpha + \vec{H}_{z_j}^k \right) w_j^k \right] \left(\sin \alpha + \vec{H}_{y_j}^k \right) \end{aligned} \quad (26)$$

5.2. Navier-Stokes Equation along z-axis

$$w_j^{k+1} = w_j^k - Re.v.\Delta t \frac{w_{j+1}^k - w_{j-1}^k}{2\Delta y} - Re.w.\Delta t \frac{w_{j+1}^k - w_{j-1}^k}{2\Delta z} + \frac{w_{j+1}^k - 2w_j^k + w_{j-1}^k}{(\Delta y)^2} +$$

$$\frac{w_{j+1}^k - 2w_j^k + w_{j-1}^k}{(\Delta z)^2} - M \cdot \left[\left(\sin\alpha + \vec{H}_{y_j}^k \right) v_j^k - \left(\cos\alpha + \vec{H}_{z_j}^k \right) w_j^k \right] \left(\cos\alpha + \vec{H}_{z_j}^k \right) \quad (27)$$

5.3. Equation of Energy

$$T_j^{k+1} = T_j^k - Re.v_j^k \Delta t \left(\frac{T_{j+1}^k - T_{j-1}^k}{2\Delta y} \right) - Re.w_j^k \Delta t \left(\frac{T_{j+1}^k - T_{j-1}^k}{2\Delta z} \right) + \frac{1}{P_r} \cdot \Delta t \left(\frac{T_{j+1}^k - 2T_j^k + T_{j-1}^k}{(\Delta y)^2} \right) + \frac{1}{P_r} \cdot \Delta t \left(\frac{T_{j+1}^k - 2T_j^k + T_{j-1}^k}{(\Delta z)^2} \right) + E_c \cdot \Delta t \left(4 \left(\frac{u_{j+1}^k - u_{j-1}^k}{2\Delta y} \right)^2 + \left(\frac{u_{j+1}^k - u_{j-1}^k}{2\Delta z} + \frac{w_{j+1}^k - w_{j-1}^k}{2\Delta y} \right)^2 \right) + \quad (28)$$

$$M.E_c \cdot \Delta t \left[\left(\sin\alpha + \vec{H}_{y_j}^k \right) v_j^k - \left(\cos\alpha + \vec{H}_{z_j}^k \right) w_j^k \right]^2 \quad (29)$$

5.4. Magnetic Induction Equation along x-axis

$$\frac{\vec{H}_{x_j}^{k+1} - \vec{H}_{x_j}^k}{\Delta t} = 0 \quad (30)$$

5.5. Magnetic Induction Equation along y-axis

$$\vec{H}_{y_j}^{k+1} = \vec{H}_{y_j}^k + Re \cdot \Delta t \left(\sin\alpha + \vec{H}_{y_j}^k \right) \left(\frac{v_{j+1}^k - v_{j-1}^k}{\Delta z} \right) + Re.v_j^k \Delta t \left(\frac{\vec{H}_{y_{j+1}}^k - \vec{H}_{y_{j-1}}^k}{\Delta z} \right) - Re \cdot \Delta t \left(\cos\alpha + \vec{H}_{z_j}^k \right) \left(\frac{w_{j+1}^k - w_{j-1}^k}{\Delta z} \right) + \frac{\Delta t}{P_{rm}} \left(\frac{\vec{H}_{z_{j+1}}^k - 2\vec{H}_{z_j}^k + \vec{H}_{z_{j-1}}^k}{(\Delta y)^2} + \frac{\vec{H}_{z_{j+1}}^k - 2\vec{H}_{z_j}^k + \vec{H}_{z_{j-1}}^k}{(\Delta z)^2} \right) \quad (31)$$

5.6. Magnetic Induction Equation along z-axis

$$\vec{H}_{y_j}^{k+1} = \vec{H}_{y_j}^k + Re \cdot \Delta t \left(\cos\alpha + \vec{H}_{z_j}^k \right) \left(\frac{w_{j+1}^k - w_{j-1}^k}{\Delta y} \right) + Re.v_j^k \Delta t \left(\frac{\vec{H}_{y_{j+1}}^k - \vec{H}_{y_{j-1}}^k}{\Delta y} \right) - Re \cdot \Delta t \left(\sin\alpha + \vec{H}_{y_j}^k \right) \left(\frac{v_{j+1}^k - v_{j-1}^k}{\Delta y} \right) + \frac{\Delta t}{P_{rm}} \left(\frac{\vec{H}_{y_{j+1}}^k - 2\vec{H}_{y_j}^k + \vec{H}_{y_{j-1}}^k}{(\Delta y)^2} + \frac{\vec{H}_{y_{j+1}}^k - 2\vec{H}_{y_j}^k + \vec{H}_{y_{j-1}}^k}{(\Delta z)^2} \right) \quad (32)$$

5.7. Equation of Concentration

$$C_j^{k+1} = C_j^k + \frac{\Delta t}{S_c} \left(\frac{C_{j+1}^k - 2C_j^k + C_{j-1}^k}{(\Delta y)^2} + \frac{C_{j+1}^k - 2C_j^k + C_{j-1}^k}{(\Delta z)^2} \right) - Re.v_j^k \cdot \Delta t \left(\frac{C_{j+1}^k - C_{j-1}^k}{2\Delta y} \right) - Re.w_j^k \cdot \Delta t \left(\frac{C_{j+1}^k - C_{j-1}^k}{2\Delta z} \right) + S_r \cdot \Delta t \left(\frac{T_{j+1}^k - 2T_j^k + T_{j-1}^k}{(\Delta y)^2} + \frac{T_{j+1}^k - 2T_j^k + T_{j-1}^k}{(\Delta z)^2} \right) - \gamma C^* \cdot \Delta t \quad (33)$$

5.8. Initial and Boundary Conditions in Finite Difference Form

From equations 26 to 33 the corresponding initial and boundary conditions in non-dimensional form are [12, 13, 14]:
Initial conditions

$$t \leq 0 : v(j, 0) = 0, w = 0, T(j, 0) = 0, C(j, 0) = 0, H_y(j, 0) = H_z(j, 0) = 0, 0 \leq (y, z) \leq 1 \quad (34)$$

Boundary conditions

$$t > 0 : \left\{ \begin{array}{ll} v(0, k) = 1, w(0, k) = 1, T(0, k) = 1, C(0, k) = 1, H_y(0, k) = H_z(0, k) = 1 & (y, z) = 0 \\ v(j, k) = 0, w(j, k) = 0, T(j, k) = 0, C(j, k) = 0, H_y(j, k) = H_z(j, k) = 0 & (y, z) = 1 \end{array} \right\} \quad (35)$$

6. Results and Discussion

In all these profiles, the value 0.2 for distance (y, z) has been used to approximate the maximum value 1 as discussed in the boundary conditions.

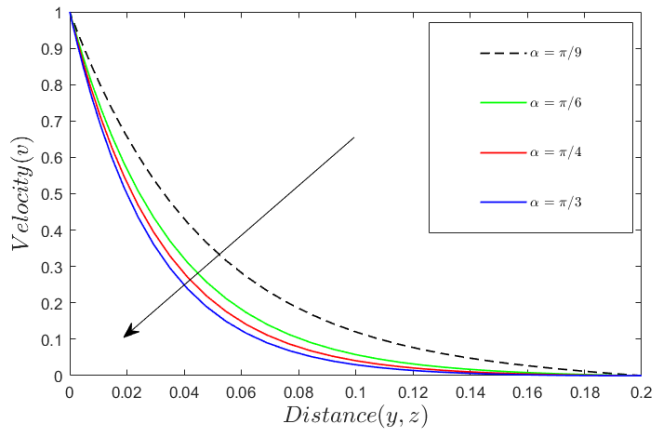


Figure 2. Velocity profiles (v) for different values of α .

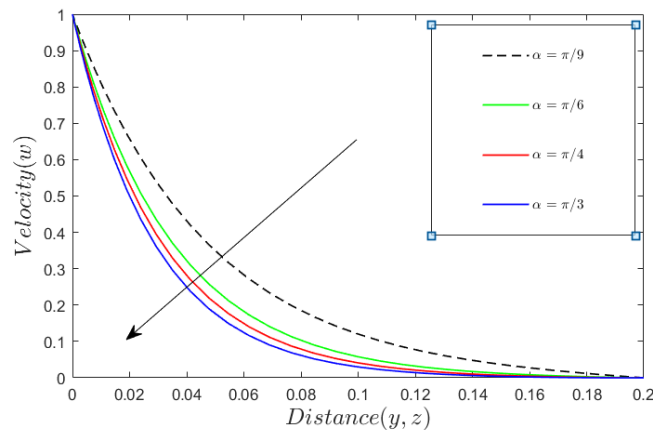


Figure 3. Velocity profiles (w) for different values of α .

Figures 2 and 3 illustrate that increasing the angle of inclination for the applied magnetic field results in a decrease in fluid velocity. This occurs because the inclined angle enhances the applied magnetic field, leading to an increase in the Lorentz force, which opposes the fluid flow. Consequently, this opposing force reduces the fluid's velocity in the flow problem.

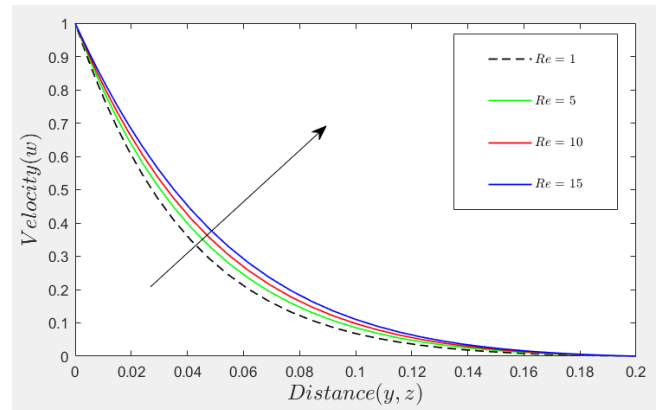


Figure 4. Velocity profiles (w) for different values of Re .

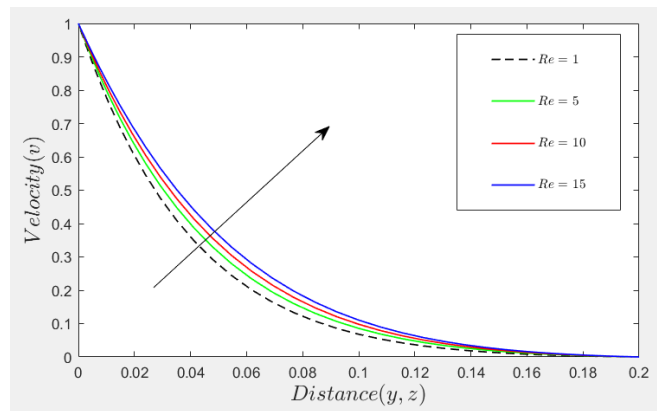


Figure 5. Velocity profiles (v) for different values of Re .

Figures 4 and 5 show that increase in the Reynolds number (Re) leads to an increase in the velocity profiles. [12] The Reynolds number represents the ratio of inertial forces to viscous forces in fluid flow. A higher Reynolds number indicates a reduction in viscous forces, allowing fluid particles to move at higher velocities due to decreased resistance. Conversely, a lower Reynolds number signifies increased viscous forces, resulting in higher resistance and consequently lower fluid velocity.

Figure 6 shows that increasing the Prandtl number leads to a decrease in the temperature of the fluid. [13] The physical significance of changing the Prandtl number lies in its impact on the heat transfer characteristics of a fluid. It influences how heat is transferred within the fluid and from the fluid to surrounding surfaces. Observations show that increasing the Prandtl number leads to a decrease in the fluid's temperature. The Prandtl number is the ratio of momentum diffusivity to thermal diffusivity. An increase in the Prandtl number reduces thermal diffusivity and increases the fluid's viscosity, which decreases the thermal boundary layer and consequently results in a lower fluid temperature.

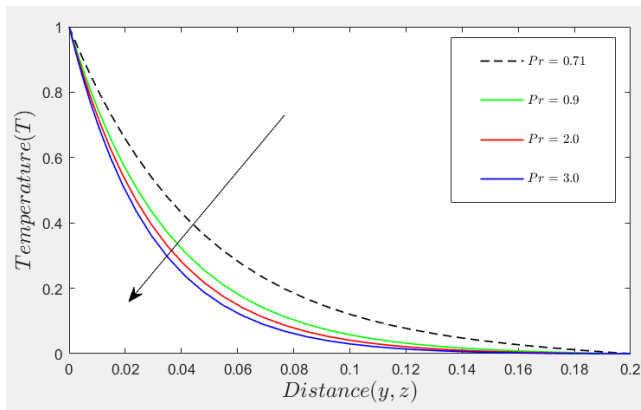


Figure 6. Temperature profiles (T) for different values of Pr .

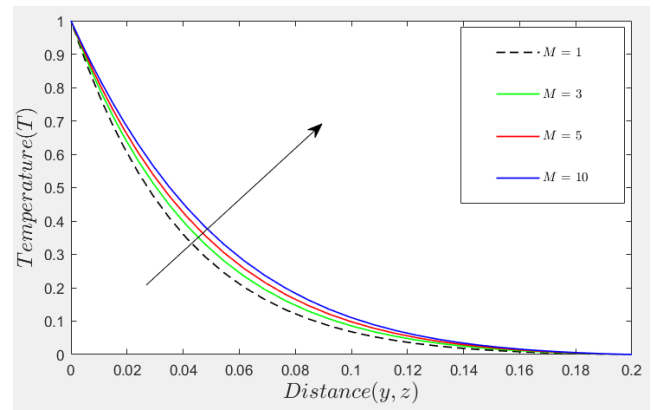


Figure 8. Temperature profiles (T) for different values of M .

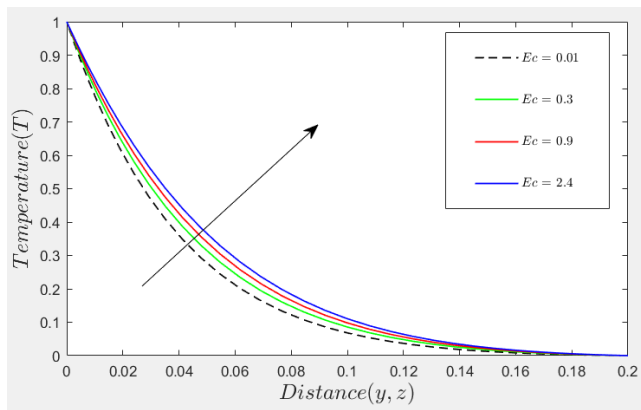


Figure 7. Temperature profiles (T) for different values of Ec .

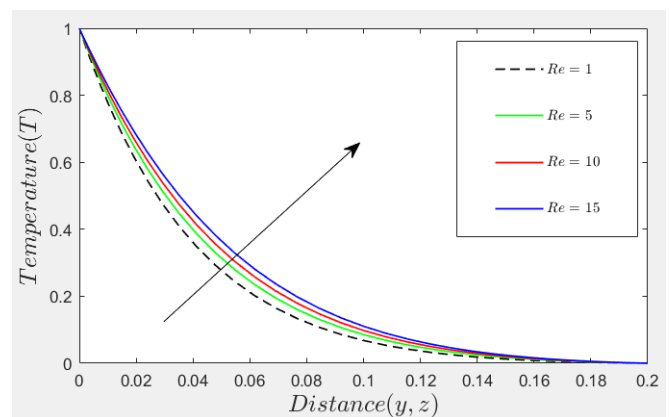


Figure 9. Temperature profiles (T) for different values of Re .

Figure 7 demonstrates that an increase in the Eckert number raises the temperature of the nanofluid. The Eckert number, being the ratio of kinetic energy to enthalpy of the nanofluid flow, indicates that as it increases, the kinetic energy of the fluid dominates over its enthalpy. This dominance leads to convective heating, as the fluid's kinetic energy is converted into thermal energy while flowing past a stretching plate. This conversion results in the production of internal energy or heat, thereby increasing the fluid's temperature [16].

Figure 8 shows that an increase in the magnetic number leads to an increase in the fluid temperature. The magnetic number, being the ratio of magnetic forces to fluid inertia forces, implies that a higher magnetic number corresponds to stronger magnetic forces and weaker inertia forces. When fluid particles in motion interact with a stronger magnetic field, this interaction induces an electric current. The fluid particles then collide with the charged particles of this current, causing vibrations that produce thermal energy in the form of heat. Consequently, increasing the magnetic number results in a rise in the fluid's temperature [13].

Figure 9 shows that increasing Reynolds number leads to an increase in the temperature profiles. Since Reynolds number is the ratio of inertia forces to viscous forces, so increasing Reynolds number implies that the viscous forces become less significant. A decrease in viscous forces means that fluid particles have increased motion and heat is generated due to collision of the particles which are moving at high velocity thereby increasing fluid temperature.

Figures 10 and 13 show that increasing magnetic Prandtl number leads to a decrease in induced magnetic field long y and z directions. Since magnetic Prandtl number is the ratio of momentum diffusivity to the magnetic diffusivity, so increasing magnetic Prandtl number implies reduction in magnetic diffusivity, which leads to decrease in the induced magnetic field by the motion of the conducting medium and thus induced magnetic profiles along y and z decrease.

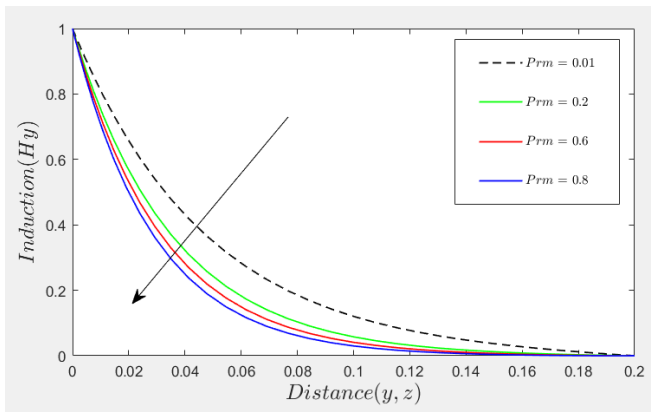


Figure 10. Magnetic Induction profiles along y (H_y) for different values of Pr_m .

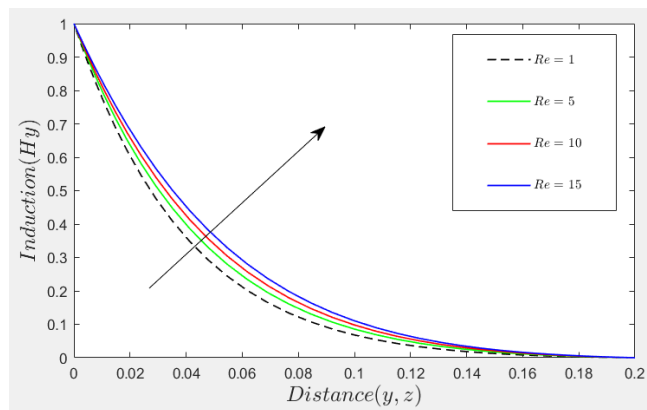


Figure 11. Magnetic Induction profiles along y (H_y) for different values of Re .

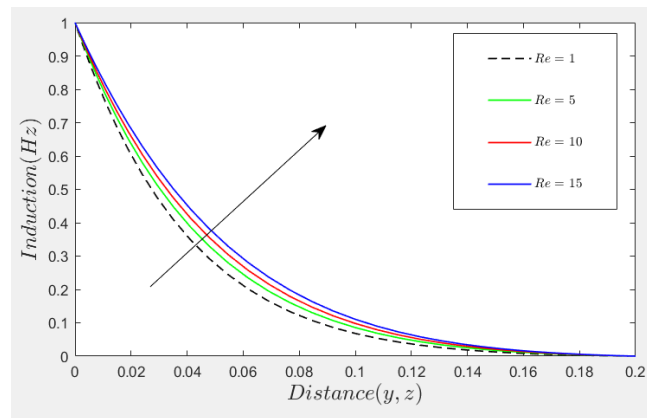


Figure 12. Magnetic Induction profiles along z (H_z) for different values of Re .

Figures 11 and 12 show that an increase in the Reynolds number leads to an increase in the induced magnetic field profiles along the y and z directions. The Reynolds number, being the ratio of inertial forces to viscous forces, implies that a higher Reynolds number corresponds to reduced viscous forces. This reduction in viscous forces enhances the interaction between the fluid and the magnetic field, thereby increasing the induced magnetic field in both the y and z directions [17].

Figure 14 shows that the concentration of the nanofluid decreases as the Schmidt number increases. The Schmidt number, being the ratio of momentum diffusivity to mass diffusivity of particles, indicates that a higher Schmidt number corresponds to reduced mass diffusivity. This reduction in mass diffusivity results in a decrease in the concentration profiles of the nanofluid.

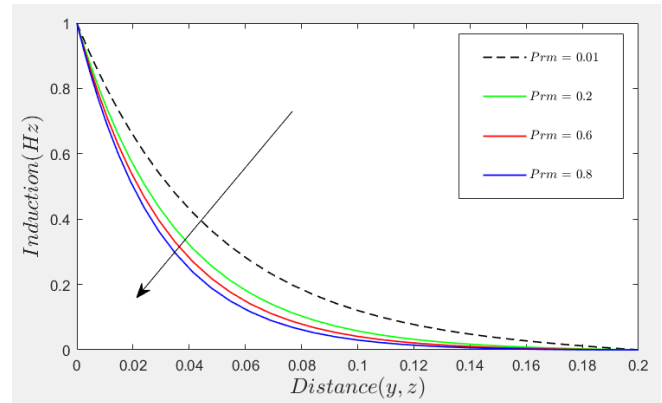


Figure 13. Magnetic Induction profiles along z (H_z) for different values of Pr_m .

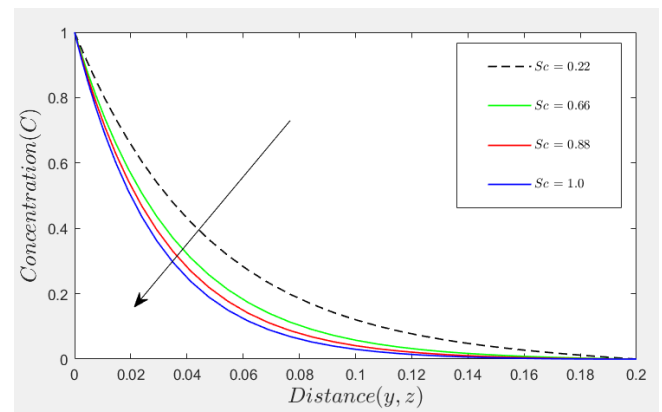


Figure 14. Concentration profiles (C) for different values of Sc .

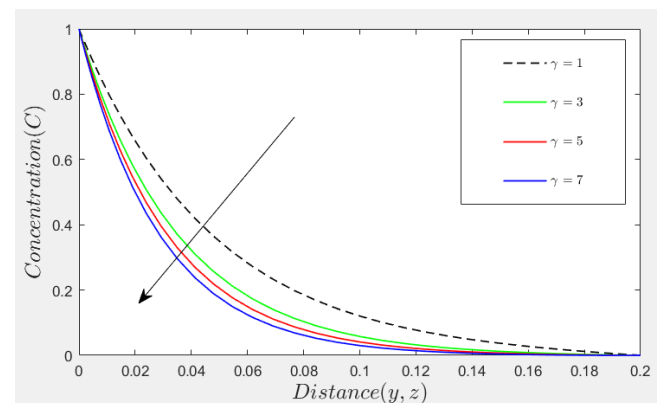


Figure 15. Concentration profiles (C) for different values of γ .

Figure 15 shows that increase in the chemical reaction parameter leads to a decrease in the concentration of the fluid particles. [15] A higher chemical reaction parameter

indicates that the chemical reaction proceeds at a faster rate relative to fluid transport. As a result, more reactants are consumed or converted into products in a given time, leading to a decrease in the concentration of the reactants in the fluid. In a chemical reaction, the concentration of reactant species decreases as they undergo chemical changes to form products. As the reaction progresses, reactant molecules collide and react, forming new products. Consequently, the concentration of the reacting species decreases because the molecules are being converted into products, leading to a decrease in chemical molecular diffusivity [14].

Figure 16 shows that increasing Soret number increases concentration profiles. [14] The Soret number determines the effect of temperature gradients on inducing significant mass diffusion effects. Increasing the Soret number generates a mass flux that leads to an increase in the mass boundary layer thickness, thereby resulting in an increase in the concentration of the fluid.

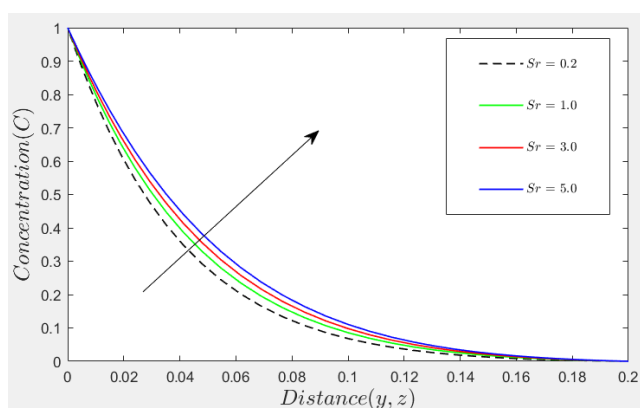


Figure 16. Concentration profiles (C) for different values of Sr .

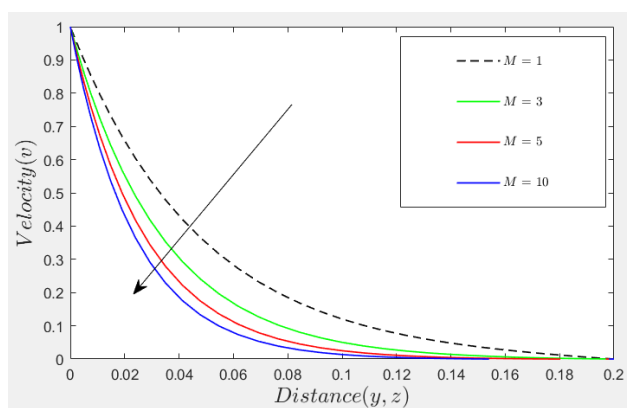


Figure 17. Velocity profiles (v) for different values of M .

In Figure 17, it is shown that increasing the magnetic number leads to a decrease in the velocity profile. This is because a higher magnetic number enhances the Lorentz force, which resists the fluid flow and thus reduces the velocity of the fluid. [12, 13].

7. Conclusion

From the results, it is observed that increasing values of Reynolds number leads to an increase in velocity profiles while increasing values of magnetic number and angle of inclination leads to decrease in the velocity profile. Increasing values of Reynolds number, Eckert number, magnetic parameter leads to increase in temperature profile while increasing the values of Prandtl number leads to decrease in temperature profile. Increasing values of Reynolds number leads to an increase in induced magnetic field profiles while increasing values of magnetic Prandtl number leads to a decrease in induced magnetic field profiles. Increasing the values of Soret number leads to an increase in concentration profiles while increasing values of Schmidt number and chemical reaction parameter leads to a decrease in concentration profile.

Abbreviations

MHD	Magnetohydrodynamics
PDE	Partial Differential Equations
ODE	Ordinary Differential Equations
FDM	Finite Difference Method
FTCS	Forward Time, Centered Space
MATLAB	Matrix Laboratory
SA	Sodium Alginate
SCMC	Sodium Carboxymethyl Cellulose
RKNM	Runge-Kutta Numerical Method
LSM	Least-Square Method
ADM	Adomian Decomposition Method
DRA	Duan-Rach Approach

ORCID

0009-0004-5176-1536 (Kafunda Tuesday)
 0000-0003-2791-6361 (Mukonda Danny)
 0000-0002-7288-287X (Mwamba Nictor)
 0000-0003-4954-3690 (Levy Kahyata Matindih)
 0000-0001-9204-6791 (Stanley Jere)

Data Availability

The data used to support the findings of this study are included within the article. The results generated using MATLAB code are presented in tables and figures and also in results and discussion of this manuscript.

Funding Statement

This research was funded by Mulungushi University, Kabwe (Zambia).

Acknowledgments

The authors acknowledge necessary efforts and contribution from each of them during the project. The authors also acknowledge Mulungushi University, Zambia for the financial support throughout this project.

Conflicts of Interest

The authors declare they have no conflicts of interest regarding publication of this article.

References

- [1] Attia, H. A., and Kotb, N. A. (1996). MHD flow between two parallel plates with heat transfer. *Acta mechanica*, 117(1), 215-220.
- [2] Ikram, M. D., Asjad, M. I., Akgül, A., and Baleanu, D. (2021). Effects of hybrid nanofluid on novel fractional model of heat transfer flow between two parallel plates. *Alexandria Engineering Journal*, 60(4), 3593-3604.
- [3] L. Lugo, J. P. Vallejo, G. Zyla, J. Fernandez-Seara Rheological behaviour of functionalized graphene nanoplatelet nanofluids based on water and propylene glycol: water mixtures *Int. Commun. Heat Mass Transfer.*, 99 (2018), pp. 43-53.
- [4] J. P. Vallejo, L. Lugo, G. Zyla, J. Fernandez-Seara Influence of Six Carbon-Based Nanomaterials on the Rheological Properties of Nanofluids *Nanomaterials*, 9 (2019), p. 146.
- [5] A. M. Rashad, A. J. Chamkha, M. Ismael, T. Salah MHD Natural Convection in a Triangular Cavity filled with a $Cu - Al_2O_3$ / Water Hybrid Nanofluid with Localized Heating from Below and Internal Heat Generation *J. Heat Transf.*, 7 (2018), p. 140.
- [6] R. Mohebbi, S. Mehryan, M. Izadi, O. Mahian Natural convection of hybrid nanofluids inside a partitioned porous cavity for application in solar power plants *J. Therm. Anal. Calorim.*, 151 (2019), pp. 154-169.
- [7] A. Shahsavari, M. Moradi, M. Bahiraei Heat transfer and entropy generation optimization for flow of a non-Newtonian hybrid nanofluid containing coated CNT/Fe_3O_4 nanoparticles in a concentric annulus *J. Taiwan Inst. Chem. Eng.* (2018), pp. 1-13.
- [8] Chu, Y. M., Bashir, S., Ramzan, M., and Malik, M. Y. (2023). Model-based comparative study of magnetohydrodynamics unsteady hybrid nanofluid flow between two infinite parallel plates with particle shape effects. *Mathematical Methods in the Applied Sciences*, 46(10), 11568-11582.
- [9] Salehi, S., Nori, A., Hosseinzadeh, K., and Ganji, D. D. (2020). Hydrothermal analysis of MHD squeezing mixture fluid suspended by hybrid nanoparticles between two parallel plates. *Case Studies in Thermal Engineering*, 21, 100650.
- [10] Dogonchi, A. S., Waqas, M., Afshar, S. R., Seyyedi, S. M., Hashemi-Tilehnoee, M., Chamkha, A. J., and Ganji, D. D. (2020). Investigation of magneto-hydrodynamic fluid squeezed between two parallel disks by considering Joule heating, thermal radiation, and adding different nanoparticles. *International Journal of Numerical Methods for Heat and Fluid Flow*, 30(2), 659-680.
- [11] Sahebi, S. A. R., Pourziaei, H., Feizi, A. R., Taheri, M. H., Rostamiyan, Y., and Ganji, D. D. (2015). Numerical analysis of natural convection for non-Newtonian fluid conveying nanoparticles between two vertical parallel plates. *The European Physical Journal Plus*, 130, 1-12.
- [12] Danny, M., Kafunda, T., Christian, K. and Stanley, J. (2024). Analysis on Heat and Mass Transfer in Boundary Layer Non-Newtonian Nanofluid Flow Past a Vertically Stretching Porous Plate with Chemical Reaction, Variable Magnetic Field and Variable Thermal Conductivity. *Int. J. Adv. Appl. Math. and Mech.* 11(4) (2024) 1-14.
- [13] Kafunda, T. et al. (2023). Unsteady hydromagnetic non-newtonian nanofluid flow past a porous stretching sheet in the presence of variable magnetic field and chemical reaction. *Journal of Applied Mathematics and Physics*, 11(9): 2545-2567.
- [14] Mwamba, N., Okelo Abonyo, J., Awuor, K. O., et al. (2023). Effects of thermal radiation and chemical reaction on hydromagnetic fluid flow in acylindrical collapsible tube with an obstacle. *International Journal of Mathematics and Mathematical Sciences*, 2023.
- [15] Ramzan, M., Inam, S., and Shehzad, S. (2016). Three dimensional boundary layer flow of aviscoelastic nanofluid with sores and dufour effects. *Alexandria Engineering Journal*, 55(1): 311-319.
- [16] Kumar, D., Singh, A., and Kumar, D. (2018). Effect of hall current on the magnetohydrodynamic free convective flow between vertical walls with induced magnetic field. *The European Physical Journal Plus*, 133(5): 207.
- [17] Yadav, A. S., Khare, R. K., and James, M. (2019). Fluid flow through porous medium in a horizontal channel in inclined magnetic field. *Journal of Applied Science and Computations*, 6(1): 1223-1226.